Results in Engineering 32 (2026) 112930

Contents lists available at ScienceDirect

Results in Engineering

journal homepage: www.sciencedirect.com/journal/results-in-engineering

Research paper

Simultaneous bisphenol A and glass fiber recovery from glass fiber-reinforced epoxy resins via NaOH-mediated alcoholysis

Carlos Marquez [a,*], Yixue Zhang [b], Karolien Vanbroekhoven [a], Marc Comi [a], Jelle Vekeman [c], Frank De Proft [d], Jan Jordens [e], Tom Rommens [f], Jan Ivens [b], Joey Abi Rizk [g], Elias Feghali [a,g,**], Kathy Elst [a]

[a] Sustainable Polymer Technologies (SPOT) Team, Flemish Institute for Technological Research (VITO), Boeretang 200, Mol, Belgium
[b] Department of Materials Engineering, KU Leuven Campus De Nayer, De Nayerlaan 5, Sint-Katelijne-Waver, 2860, Belgium
[c] Modelling and Simulation in Chemistry (MOSAIC), University of Antwerp, Groenenborgerlaan 171, Antwerpen, 2020, Belgium
[d] Research Group of General Chemistry (ALGC), Vrije Universiteit Brussel (VUB), Pleinlaan 2, Brussels, B-1050, Belgium
[e] Specialized Analysis Team (GOAL), Flemish Institute for Technological Research (VITO), Boeretang 200, Mol, Belgium
[f] Assessment & Development of Value Networks Team (ADVANCE), Flemish Institute for Technological Research (VITO), Boeretang 200, Mol, Belgium
[g] Chemical Engineering Program, Notre Dame University-Louaize, Zouk Mosbeh, 1211, Lebanon

ARTICLE INFO

Keywords:
Epoxy resin depolymerization
Methanolysis
Bisphenol A recovery
Fiber-reinforced composites
Glass fiber recovery
Wind turbine blades
Life cycle assessment

ABSTRACT

The limited recyclability of thermoset epoxy resins in fiber-reinforced composites presents a growing environmental challenge, particularly for the recovery of bisphenol A (BPA) from bisphenol A diglycidyl ether (BADGE)-based systems. Herein, we report an efficient depolymerization strategy based on a NaOH-mediated alcoholysis process. This approach represents a conceptual departure from current epoxy deconstruction strategies, which typically rely on either transition-metal catalysis or harsh acidic/alkaline conditions. Using an inexpensive and readily available base, BPA is recovered in yields of up to 90% under relatively mild conditions and short reaction times. Mechanistic analysis combining experiments and molecular dynamics reveals that polymer structure, particularly the type of amine curing agent, governs accessibility of catalytically active species and overall reactivity, with more flexible networks enabling enhanced accessibility to the polymer chains. The process is successfully extended to glass fiber-reinforced composites and real end-of-life wind turbine blades, enabling simultaneous recovery of both BPA and glass fibers, which retain mechanical properties comparable to virgin materials. Importantly, beyond monomer recovery, this work establishes a direct link between polymer network structure and depolymerization efficiency via combined experimental and molecular simulation insights, providing a previously underexplored framework for understanding thermoset deconstruction. A life cycle assessment (LCA) further demonstrates the potential of this approach as a base-mediated route to thermoset deconstruction with reduced environmental impact in comparison to current composite waste management practices, highlighting its potential for scalable implementation.

1. Introduction

Thermoset epoxy resins are polymers prepared by blending a component bearing an epoxy function (usually bisphenol A-based, BPA) with a curing agent (amines or anhydrides) [1]. Unlike thermoplastics (like polycarbonate or polyvinyl chloride), these thermosets are not considered recyclable, due to the (strong) covalent bonds formed during the curing process forming a heavily cross-linked 3D network. Epoxy resins are widely used in construction, electronic and manufacturing applications as coating and adhesives for structural and other purposes. However, their major application is undoubtedly in fiber-reinforced epoxy composites [2]. Epoxy resins comprise ~50 wt% of carbon fiber or ~40 wt% of glass fiber composite materials [2–4]. Carbon fiber reinforced polymer (CFRPs) composites have been extensively used in the aerospace, transport, marine and wind energy sector for more than five decades. The annual growth rate of CFRPs is about 12.5% over the

* Corresponding author.
** Corresponding author at: Sustainable Polymer Technologies (SPOT) Team, Flemish Institute for Technological Research (VITO), Boeretang 200, Mol, Belgium.
E-mail addresses: carlos.marquezadmade@vito.be (C. Marquez), elias.feghali@vito.be (E. Feghali).

https://doi.org/10.1016/j.rineng.2026.112930
Received 30 June 2026; Received in revised form 7 September 2026; Accepted 9 September 2026
Available online 10 September 2026
2590-1230/© 2026 The Authors. Published by Elsevier B.V. This is an open access article under the CC BY-NC license (http://creativecommons.org/licenses/by-nc/4.0/).

last two decades, with a global demand of 4 million metric tons in 2020 [5–10]. On the other hand, glass fiber reinforced polymer (GFRP) composites find applications across diverse engineering fields and are the preferred material for wind turbine blade skin manufacturing, representing a rapidly expanding market. It is estimated that approximately 550,000 tonnes of epoxy are used annually worldwide for wind turbine blades, with around 40,000 tonnes consumed in Europe alone. Nevertheless, recycling solutions for end-of-life (EOL) composite materials are critically underdeveloped, while the amount of EOL GFRP wind turbine blades alone is expected to reach around 30 kT per year between 2020 and 2030 [4,11–15].

The most common disposal methods for composite waste involve landfilling, co-processing in cement kilns, pyrolysis, or mechanical recycling by grinding composites for use in applications that can tolerate lower-quality mechanical properties [16–20]. Even though emerging chemical recycling strategies primarily focus on recycling of fibers [21, 22], the epoxy portion of these composites also represents a substantial amount of unrecovered carbon [2,3]. Together with an increasing concern over BPA's environmental and health effects, this has led to a growing demand for effective methods to recover and recycle BPA from thermoset epoxy resins. Traditional methods of BPA recovery often involve complex processes that can be time-consuming and require significant amounts of chemical reagents, which may not be environmentally friendly.

In recent years, significant progress has been made in the chemical recycling of thermoset epoxy resins (Fig. 1, Table S1). These approaches can be categorized into transition metal-catalyzed degradation, alkali-mediated depolymerization and organic acid solvolysis. Transition metal-catalyzed systems, such as those developed by the groups of Skrydstrup and Nozaki, have demonstrated good BPA recovery yields through efficient cleavage of epoxy networks [23–25]. However, these catalytic systems are generally expensive and can be sensitive to oxygen, moisture, and feedstock impurities, potentially limiting large-scale implementation. Alkali-mediated depolymerization has emerged as another effective strategy for epoxy deconstruction. High BPA recoveries can be achieved through cleavage of ether linkages within the polymer network; however, these methods often require large amounts of corrosive bases and/or elevated temperatures, creating challenges related to process safety, equipment corrosion, waste treatment, and overall economic viability [11,26]. Organic acid-based solvolysis represents an alternative approach. Recently, Beckham et al. [27] demonstrated efficient recovery of BPA and reinforcing fibers from GFRP composites using acetic acid. While promising, acid-mediated processes may require substantial solvent consumption, extended treatment times, and can potentially affect fiber quality or downstream processing depending on the operating conditions employed. Collectively, these studies demonstrate the feasibility of recovering BPA from thermoset epoxy resins, yet important limitations remain. Furthermore, most studies focus primarily on BPA yield and catalyst development, while the influence of polymer network structure on reagent accessibility and depolymerization performance remains insufficiently understood. In contrast, the present system demonstrates that efficient depolymerization can be achieved without recourse to complex catalytic systems, instead highlighting that catalyst accessibility within the polymer network can be as critical as intrinsic catalytic activity.

As industries transition toward more sustainable materials management, there is a growing need for recycling strategies that can recover value from thermoset epoxy resins and composites while minimizing environmental impact and resource use [28–31]. From both scientific and engineering perspectives, two key challenges remain unresolved: (i) the development of depolymerization processes capable of recovering BPA efficiently under mild and industrially relevant conditions, and (ii) the establishment of a mechanistic understanding of how curing-agent chemistry and polymer network architecture govern catalyst accessibility, bond cleavage, and overall depolymerization efficiency. Addressing these challenges is essential for designing scalable recycling technologies capable of handling the diverse epoxy composite waste streams generated by modern industries. While most existing approaches are often limited by harsh conditions, narrow applicability across resin/curing agent chemistries, or incomplete valorization of composite components, here, we report a base-mediated methanolysis platform for epoxy depolymerization that enables recovery of BPA under mild conditions. Beyond monomer recovery, we elucidate how the nature of industrially relevant amine curing agents governs depolymerization efficiency, combining experimental results with molecular dynamics simulations to investigate catalyst accessibility and uncover structure-reactivity relationships within the polymer network for the first time. Taken together, these elements distinguish the present work from prior studies by integrating reaction engineering, structure-reactivity relationships, and materials recovery into a unified framework, rather than focusing solely on catalytic performance or monomer yields. These results highlight that thermoset deconstruction is governed not only by reactivity of chemical bonds but also by catalyst speciation and accessibility within the polymer network. The method is further evaluated for application to glass fiber-reinforced composites, and its environmental implications are assessed through life cycle analysis. As such, this work goes beyond incremental improvements in depolymerization efficiency and instead introduces a more generalizable strategy for thermoset deconstruction that couples molecular-level understanding with practical composite recycling.

2. Results and discussion

2.1. Base-mediated alcoholysis of amine-cured epoxy resins

2.1.1. Optimization of base loading

In assessing the possible depolymerization of thermoset epoxy resins using alcoholysis, we evaluated the effect of NaOH loading in the base-

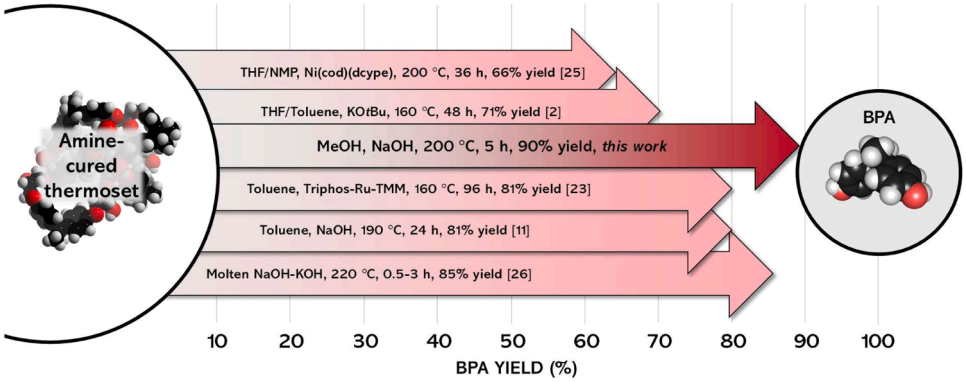


Fig. 1. Summary of chemical recycling strategies for amine-cured epoxy resins for BPA recovery.

mediated methanolysis of a home-made epoxy resin based on diglycidyl ether of bisphenol A (BADGE) and JEFFAMINE D-230 polyetheramine (JEFFAMINE), as curing agent. The first set of reactions were conducted at 200 °C, varying both the NaOH loading and the reaction time (Fig. 2a, Table S4). Excellent BPA yields were obtained under several conditions, reaching a maximum of 90 ± 8% when the reaction was carried out for 24 h with 50 wt% of base. Notably, good yields were obtained at reduced reaction times and lower NaOH loadings as well. For instance, 25 wt% NaOH resulted in a BPA yield of 50 ± 5% after only 5 h, which increased to 62 ± 8% after 24 h. Similarly, 20 wt% NaOH gave 57 ± 9% yield after 5 h, suggesting that high BPA recovery yields can be achieved under milder conditions. In contrast, sub-stoichiometric NaOH amounts led to significantly lower BPA yields (e.g., 34 ± 4% with 10 wt% of NaOH after 24 h), indicating the importance of sufficient base loading for effective depolymerization. This strong dependence on base loading suggests limitations in effective catalyst concentration, likely arising from restricted diffusion and local accessibility within the crosslinked network. Notably, in the absence of NaOH depolymerization does not occur, even at higher temperatures, highlighting the essential role of base-derived reactive species in bond cleavage (Table S5). Accordingly, 20 wt% NaOH and a 5 h reaction time were chosen as baseline conditions for subsequent optimization studies. Under these conditions, depolymerization yields (in addition to the recovered monomer) a complex and highly polar residual fraction. Previous solvolysis studies on related thermosets and thermoplastics have described this fraction as a mixture of oligomeric species containing alkyl esters, amines, and aromatic units; however, detailed structural identification of the larger compounds has remained elusive.[2,11] In this work, HPLC-MS analysis enabled the elucidation of potential structures within this fraction, which could be classified into four groups according to the number of biaryl (i.e., BPA) moieties present: species containing no BPA units, one BPA unit, two BPA units, and more than two BPA units (Figs. S7–S11). These results are consistent with our hypothesized reaction network (Scheme S1), in which the epoxy resin initially fragments into heavy oligomers that are subsequently converted into smaller trimers and dimers as the reaction progresses, ultimately leading to the release of BPA.

2.1.2. Solvent screening

Since these initial experiments demonstrated the prospect of depolymerization of BPA-based thermoset epoxy resins using methanolysis, we further tested the possibility of expanding the alcoholysis to other short-length alcohols. As shown in Table S6 and Fig. S2, lower alkyl alcohols, like ethanol and 2-propanol, can effectively break down the polymer network to obtain excellent epoxy conversions and BPA yields in similar values as with methanol. Notably, the reaction does not proceed when aprotic solvents (e.g. THF, toluene, dioxane) are used instead, demonstrating the importance of alcohols as efficient depolymerization reagents of the resin.

2.1.3. Comparison of different inorganic bases

Encouraged by the promising results obtained with NaOH, we subsequently screened a series of alkali and alkaline earth hydroxides as promoters for epoxy resin deconstruction (Table S7). Unlike other recent base-promoted polymer deconstruction processes, where KOH and KO*t*Bu also showcased a respectable activity [2,11], our screening revealed a markedly superior activity for NaOH (Table S7), achieving almost full epoxy conversion (liquefaction) and high BPA yields under mild reaction conditions. In contrast, only moderate epoxy conversion (<61%) were obtained with all the other bases. These results can most likely be explained by the differences in solubility of the various bases in methanol. In this regard, NaOH is known to exhibit a greater solubility in methanol than other hydroxides, leading to a higher concentration of reactive hydroxide (or methoxide) species in solution. Contrary to previous reports on base-mediated epoxy resin deconstruction processes [11], our results suggest that an enhanced solubility of the base facilitates a more efficient cleavage of the polymer network, which is further supported by the fact that no epoxy conversion is observed when aprotic solvents (not able to solubilize NaOH) are employed (vide supra).

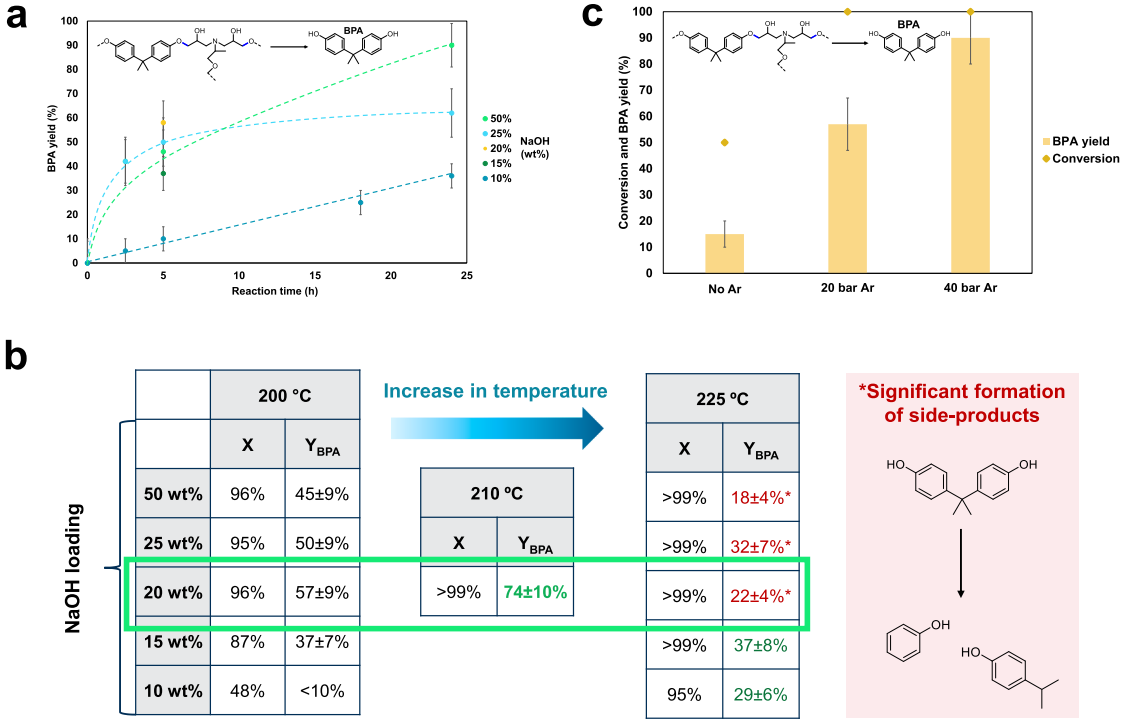


Fig. 2. Base promoted methanolysis of amine-cured epoxy resins. a Effect of NaOH as a promoter in the BPA yield obtained in the methanolysis of epoxy resins (reaction conditions: 200 °C, 5 wt% polymer loading and 20 bar Ar). **b** Effect of temperature in the methanolysis of epoxy resins (reaction conditions: 20 wt% NaOH, 5 h, 5 wt% polymer loading and 20 bar Ar). **c** Effect of Ar pressure in the methanolysis of epoxy resins (reaction conditions: 200 °C, 20 wt% NaOH, 5 h and 5 wt% polymer loading). Values represent mean ± standard deviation from two independent measurements.

Although the reaction formally proceeds via base-mediated alcoholysis, the active species are likely hydroxide and methoxide ions in solution. To further investigate the nature of the active depolymerization species, sodium methoxide (NaOMe) was evaluated under otherwise identical reaction conditions (Table S7). Remarkably, NaOMe afforded a BPA yield of 51 ± 8%, comparable to the one obtained using NaOH. The similar performance observed with the two bases suggests that methoxide species actively participate in the depolymerization process, supporting our hypothesis, although the precise contribution of each nucleophile remains difficult to distinguish under the present conditions. Furthermore, under the reaction conditions, a significant fraction of the base may be sequestered as phenolate salts or ion-paired species, effectively lowering the concentration of catalytically active species. Restricted diffusion and limited swelling also reduce accessibility of reactive hydroxide/methoxide species to internal C(alkyl)-O bonds, such that depolymerization rates are governed by effective local concentrations rather than bulk composition. As a result, relatively high NaOH loadings are required to sustain efficient depolymerization. Increasing NaOH loading therefore compensates for both chemical sequestration and physical accessibility constraints. Compared with recent epoxy depolymerization strategies based on transition-metal catalysts [23–25], the present approach achieves excellent BPA recoveries using a simple commodity base rather than specialized catalytic systems.

2.1.4. Effects of temperature and pressure

As previously mentioned, one of the main drawbacks of the proposed epoxy resin depolymerization protocols are the long reaction times needed to afford decent BPA yields. Based on our preliminary results where a BPA yield of 58 ± 7% after only 5 h was achieved, we were persuaded to further optimize the reaction conditions (i.e. reaction temperature and pressure) to maximize the BPA recovery. First, the effect of reaction temperature was evaluated at different NaOH loadings (Fig. 2b). It can be observed that at NaOH loadings >20 wt% an increase from 200 to 225 °C results in a decrease in BPA yield, due to the formation of smaller phenolic compounds, indicative of competing base-mediated side reactions at elevated temperatures, as a result of the decomposition of the BPA molecule (phenol and 4-isopropylphenol). Remarkably, at an intermediate temperature of 210 °C, a BPA yield of 74 ± 10% is obtained with 20 wt% of NaOH as promoter (Fig. S3). Since the reaction is carried out in an inert atmosphere, the effect of Ar pressure was also studied. As observed in Fig. 2c, when the reaction was carried out after just flushing with Ar (autogenous pressure), the epoxy conversion halved, in comparison to our baseline conditions. Remarkably, an increase in the Ar pressure to 40 bar, was found to enhance the yield of BPA, reaching an outstanding 90 ± 9% after 5 h of reaction time. Although Ar is chemically inert and naturally does not participate in the reaction, its elevated partial pressure and presence in the reactor headspace appears to influence the reaction system. Higher Ar pressures might suppress the volatilization of methanol, which functions as both reagent and solvent in the process. By limiting methanol loss to the gas phase, a greater proportion of the alcohol remains in the liquid, where it can effectively participate in the depolymerization reaction, enhancing reagent availability, thereby contributing to the increased production of BPA. These observations suggest that alternative process configurations capable of maintaining similar methanol partial pressures, such as operation at higher filling ratios and autogenous pressure, may provide comparable benefits while reducing gas-compression requirements. Evaluation of such strategies remains the subject of future work.

2.1.5. Depolymerization of epoxy resins cured with different amines

After establishing the optimal conditions to conduct our depolymerization protocol, we extended the methanolysis to a series of thermoset resins based on bisphenol A (BPA) and bisphenol F (BPF), cured with different amine-based agents. This allowed us to evaluate the general applicability of the method and how resin composition affects reactivity. Comparison of the results obtained with the resins derived from the two diglycidyl ether precursors revealed only marginal differences in reactivity, well within the experimental margin of error (Table S8). In contrast, replacing JEFFAMINE D-230 polyetheramine with other diamines as curing agents, namely isophorone diamine (IPDA, a commonly used cycloaliphatic epoxy hardener) and m-xylylenediamine (m-XDA) [32,33], led to more noticeable differences in reactivity. As observed in Fig. 3a, under our standard reaction conditions, the conversion (or epoxy resin liquefaction) remained below 70% when IPDA and m-XDA were used as hardeners. It is important to note, however, that an increase in the base loading to 50 wt% resulted in full resin conversion and a substantial surge in the BPA and BPF yields, regardless of the hardener or diglycidyl ether precursor used (Table S9). These differences can be attributed to the specific resin structures, which affect the accessibility of the targeted C(alkyl)-O bond. In the case of the JEFFAMINE-cured resin, the longer, linear polyetheramine chain provides more space (less steric hindrance), facilitating the nucleophilic attack on the bond and resulting in higher reactivity compared to IPDA- and m-XDA-cured resins.

2.2. Molecular insights into accessibility of reactive species and depolymerization pathways

To confirm that the longer, linear polyetheramine chain provides more space within the JEFFAMINE-cured resin, molecular dynamics simulations were performed on BADGE-based resins cured with JEFFAMINE (BPA-JEFF), IPDA (BPA-IPDA), and m-XDA (BPA-mXDA). The simulations were used to assess how the curing-agent structure affects the accessibility of the C(alkyl)-O bonds in the resulting epoxy networks. To keep the computational cost reasonable, tetramers were used (see Fig. 3b) rather than full epoxy networks which will influence molecular flexibility and accessibility of the reaction sites. More specifically, the tetramers are expected to display increased flexibility over 3D networks, yet there is no reason to believe that the qualitative trends should be any different. Furthermore, the curing of epoxy resins is inherently heterogeneous featuring regions with high and low crosslinking density [34,35]. Following the proposed reaction mechanism in Scheme S1, initial breakup of the network is likely to occur in low density regions with high accessibility and flexibility. As a result, we deem the considered tetramers to be suitable models for regions of the mesh with high flexibility as well as the heavy oligomers that occur in later stages of the breakdown process as discussed above. Note further that the simulations are only aimed at assessing accessibility and do not model reactivity itself and therefore do not include the catalyst itself, which is motivated by the observation that the reactive site is very similar for the three considered resins.

A visual inspection of the simulation trajectories reveals that all three epoxy resins switch easily and frequently between compact and stretched conformations, as shown in both ball-and-stick and solvent contact surface representations (Fig. 3b and Fig. S12). This is confirmed numerically through calculation of their radii of gyration (Rg, which represents the compactness of a molecule as schematically represented in Fig. 3b) throughout the different simulations as shown in Fig. 3c. This finding suggests a delicate interplay between intramolecular interactions within the epoxy resin and interactions with the solvent that govern the configuration of the tetramer. Averaged over the trajectories, the Rg of BPA-JEFF (1.02 nm) was found to be significantly larger than the Rg of both BPA-IPDA (0.90 nm) and BPA-mXDA (0.92 nm), which confirms that the linear curing agent leads to more extended conformations. Furthermore, the distributions of the observed radii (Fig. 3d) show that the lower-bound values are very similar for the three tetramers, yet only BPA-JEFF has access to more extended configurations. This means that it has the flexibility to visit similar collapsed states as BPA-IPDA and BPA-mXDA but also has access to extended states that are not accessible to the latter two. This is important since it is very likely that the depolymerization reaction occurs in the extended state when

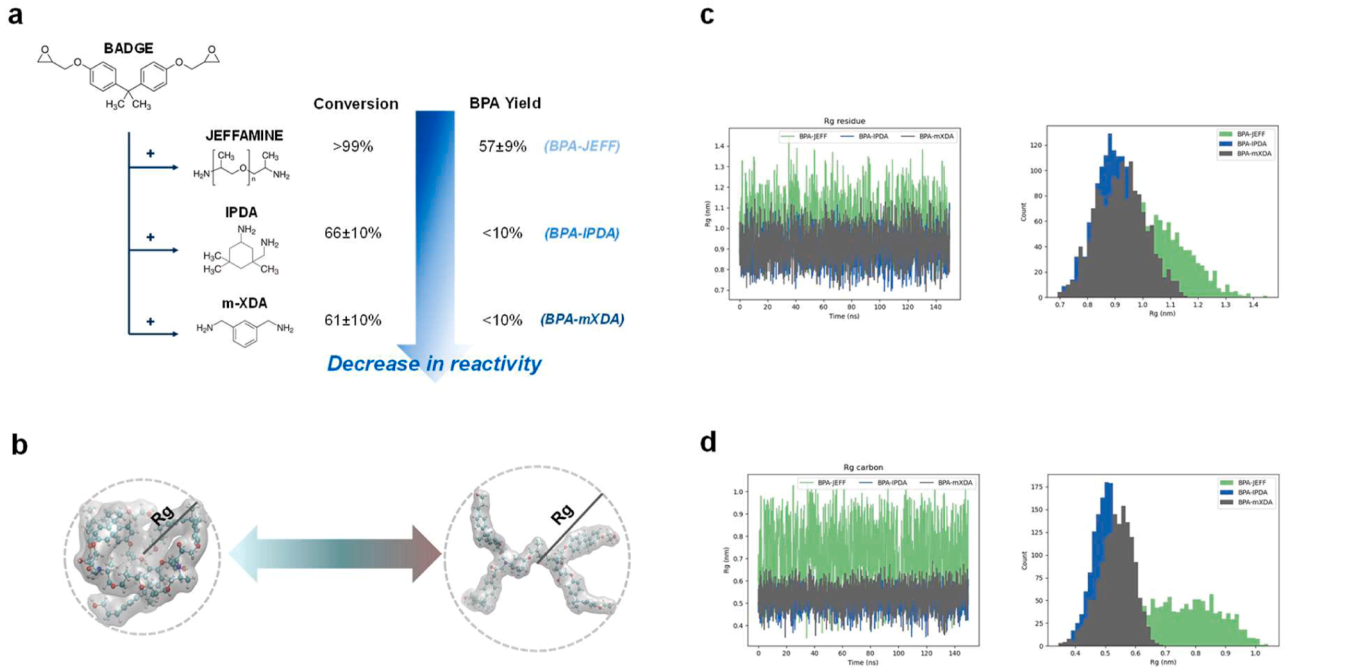


Fig. 3. Reactivity of different epoxy resins. a Conversion and BPA yield obtained from each BADGE-curing agent combination (reaction conditions: 200 °C, 5 h, 5 wt.% polymer loading, 20 wt% NaOH and 20 bar Ar). Values represent mean ± standard deviation from two independent measurements **b** Compacted (left) and stretched (right) conformation of BPA-JEFF. **c** Radii of gyration (Rg) for the different epoxies. **d** Rg values for the different epoxies, considering only C atoms of interest. Lower Rg correspond to a compact network with closely packed chains and limited free volume, restricting penetrant diffusion. Higher Rg correspond to a more expanded network with larger free-volume, facilitating transport and accessibility. Thus, increasing Rg can be interpreted as an indicator of enhanced network accessibility.

the C(alkyl)-O bonds in the epoxy resin atoms are most accessible to the solvent and the catalyst. It is noteworthy that no clearly separated collapsed and extended conformations are observed, but rather a continuum of Rg values.

To further assess specifically the carbon atoms of interest for the studied depolymerization reaction, their Rg were assessed where the 4 carbon atoms were treated as if they were a single molecule. This is different from the general Rg of the molecule since the carbons of interest are located relatively close to the center of the molecule, in a section that is less exposed to the solvent in comparison to the outer ends of the tetramers. As such, this partial Rg gives an indication of the extent to which the relevant carbons are separated from each other and the center of mass of this (in principle) symmetric molecule and thus accessible to the solvent. The trends of the general Rg are significantly enlarged when considering just the carbon atoms of interest with an Rg of 0.71 nm for BPA-JEFF, compared to BPA-IPDA (0.50 nm) and BPA-mXDA (0.54 nm). Thereby, the standard deviations of the observed Rg throughout the trajectories are substantially higher for BPA-JEFF than for the BPA-IPDA and BPA-mXDA resins with values of 0.149 (which amounts to a standard deviation of about 21%), 0.046 (~9%) and 0.057 (~11%), respectively. Interestingly, from the Rg distribution it is now clearly visible that the C atoms of interest visit different states for the three epoxides. Whereas BPA-IPDA and BPA-mXDA display a rather narrow distribution, it is much broader for BPA-JEFF and has no clear peak. These findings show that the carbons of interest (which are located close to the rigid center of the molecule) are very restricted in their movements for the tetramers with rigid linkers. On the contrary, the flexible, long chain of JEFFAMINE D-230 polyetheramine enables the C(alkyl)-O bonds on BPA-JEFF to explore the conformational space much more broadly and visit conformations with enhanced access to the solvent and catalyst. Given that small changes in accessibility can lead to major differences in reaction rates, this provides strong support for a structure-reactivity relationship in which polymer flexibility governs accessibility of reactive species and depolymerization efficiency. While the present results strongly support the importance of accessibility and mass transport within the polymer network, they do not allow complete separation of diffusion-controlled effects from kinetics-controlled effects. Because the same C(alkyl)-O bonds are targeted in all investigated resins, the observed differences in depolymerization performance are most likely attributed to variations in accessibility and conformational flexibility. A rigorous distinction between accessibility and intrinsic bond reactivity would require dedicated kinetic analysis and/or quantum-chemical studies, which fall beyond the scope of the present work. Furthermore, the diffusion resistance of bulk networks might differ quantitatively from the currently considered linear oligomeric chains, yet the observed trends are expected to be the same in regions with low crosslinking density as well as in heavy oligomers.

2.3. *Glass fiber recovery from GFRPs*

The scope of the base-mediated depolymerization process was extended to composite materials, specifically to GFRPs. To this end, a model GFRP was synthesized via vacuum-assisted resin infusion using a BPA-based epoxy resin and a 1,2-diaminocyclohexane hardener (see Supplementary Information for details). Depolymerization under our optimal conditions led to complete liquefaction of the epoxy matrix, enabling 60±8% recovery of BPA and a facile isolation of the glass fibers by simple filtration. Given the importance of solids loading for process intensification and environmental performance, additional depolymerization experiments were conducted at 20 and 50 wt% GFRP loadings under otherwise identical reaction conditions. As shown in Table S10, BPA recovery remained at 48 ± 4% and 24 ± 6% for 20 and 50 wt% loadings, respectively. To evaluate potential effects on fiber cleanliness, the recovered fibers were analyzed by thermogravimetric analysis. Residual contents of 3.9 ± 1.1 wt% and 6.9 ± 2.1 wt% were measured for fibers recovered at 20 and 50 wt% loading, respectively, indicating that depolymerization and full matrix removal remains feasible at substantially higher feed concentrations.

Since glass fibers constitute the dominant fraction of GFRPs, their intact recovery is particularly beneficial for lowering production costs and reducing resource consumption. The recovered glass fibers (rGF) were subsequently characterized and benchmarked against virgin glass fibers (vGF), with particular attention to surface condition, residual contamination, and retention of mechanical properties. In addition, a subset of rGF was subjected to ultrasonic washing in acetone (rGF-washed) to evaluate whether post-treatment cleaning could further improve fiber cleanliness and performance. First, surface morphology was examined by SEM (Fig. 4). The vGF displayed a smooth and clean surface, characteristic of fibers with an intact sizing layer (Fig. 4a). In contrast, the rGF exhibited discrete surface deposits distributed along the fiber length (Fig. 4b). EDS analysis revealed a higher Na signal in rGF compared to vGF (Fig. 4c), indicating the presence of sodium-rich residues, likely originating from the NaOH-derived precipitation upon cooling during methanolysis. Notably, no significant carbon signal was detected in the rGF spectra, confirming effective removal of the epoxy matrix. After ultrasonic washing in acetone (rGF-washed), the surface became markedly cleaner, with most deposits removed (Fig. 4d). Although glass fibers are susceptible to alkaline degradation [36,37], no severe surface pitting or etching was observed under the applied methanolysis conditions. Residual content was assessed by thermogravimetric analysis (TGA) and burn-off tests. The TGA curves (Fig. 4e) show minimal mass loss for the vGF, consistent with their inorganic nature, while the pure epoxy exhibits a complete degradation between ~300 and 450 °C (Fig. S13). In comparison, the rGF displays only a marginally higher mass loss over the same temperature range (~1 wt% higher), indicating the presence of trace residual species. Burn-off measurements (Fig. 4f) further support this observation, with rGF exhibiting a slightly higher weight loss (1.7 ± 0.2 wt%) compared to vGF (0.8 ± 0.2 wt%). Importantly, this difference remains minor and does not indicate significant contamination. Moreover, after a simple acetone washing step, the weight loss decreases to 1.0 ± 0.3 wt%, comparable to the vGF baseline, confirming that these trace surface residues are readily removed. This corroborates SEM observations and confirms the effectiveness of the laboratory-scale cleaning treatment used here.

Fig. 5 presents the tensile strength, Young's modulus, fibre diameter, and strain at failure of vGF, rGF, and rGF-washed at gauge lengths of 4, 12, and 20 mm. Statistical significance was evaluated using one-way ANOVA with Tukey's post-hoc test; groups sharing the same letter are not significantly different ($p > 0.05$). The corresponding mean values and standard deviations are summarized in Figs. S14–S16. As expected for brittle fibers, all three groups showed a decrease in tensile strength with increasing gauge length, consistent with Weibull weakest-link

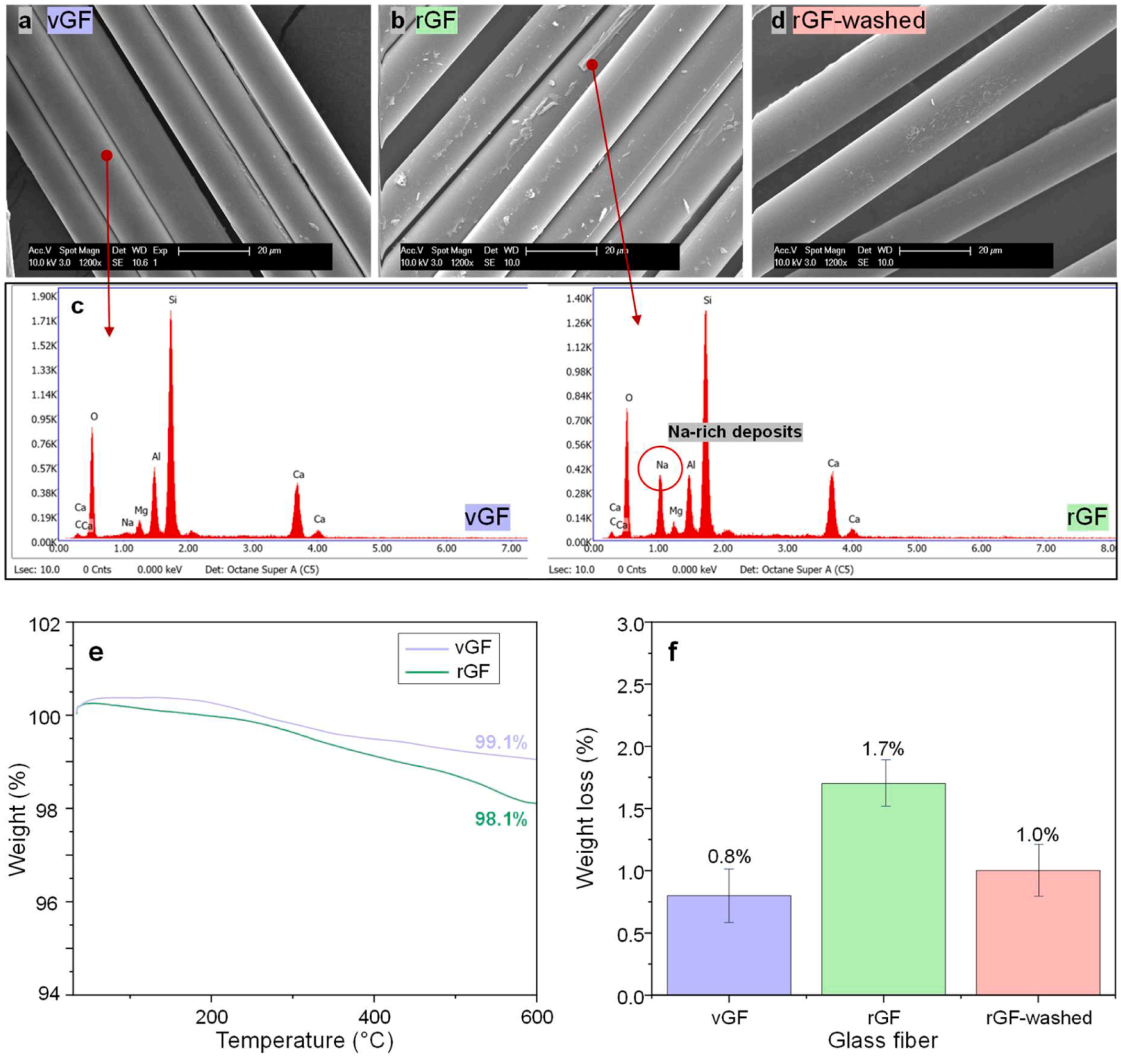


Fig. 4. SEM images, EDS spectra and thermal analysis of glass fibers before and after methanolysis. a SEM image of vGF: smooth surface with intact sizing. **b** SEM image of rGF: a more irregular surface with small deposits after methanolysis. **c** EDS spectra of vGF and rGF: identifying Na-rich deposits. **d** SEM image of rGF-washed: clean surface after ultrasonic washing in acetone. e TGA curves of vGF and rGF. f Residual weight loss of vGF, rGF, and rGF-washed from burn-off tests. Values represent mean ± standard deviation from three independent measurements.

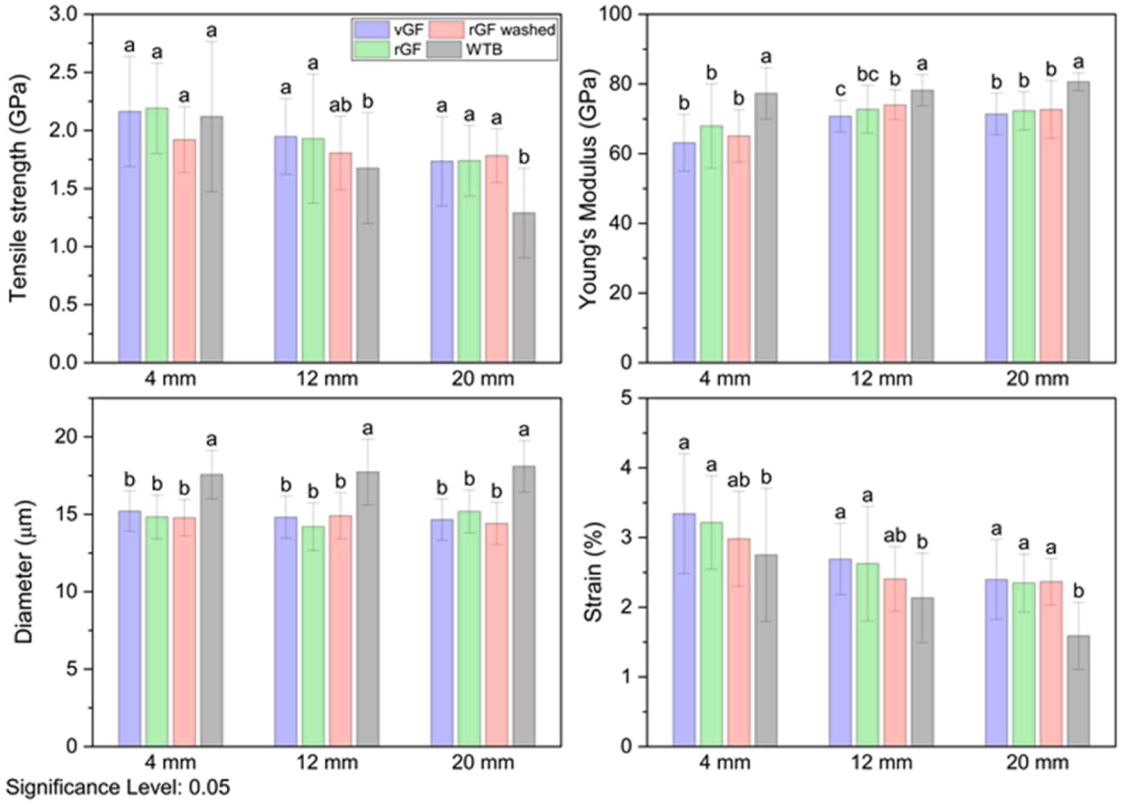


Fig. 5. Single-fiber tensile properties of vGF, rGF, rGF washed, and rGF from a decommissioned WTB at gauge lengths of 4, 12, and 20 mm. a Tensile strength. **b** Young's modulus. **c** Fiber diameter. **d** Strain at failure. Error bars represent standard deviation. Different letters indicate statistically significant differences between groups at the same gauge length (Tukey's post-hoc test, $p < 0.05$).

behavior. This dependence arises because longer gauge lengths sample a larger volume and therefore have a higher probability of containing critical flaws that initiate fracture [38,39]. The measured vGF strength of 1.95 GPa at 12 mm is consistent with values reported in the literature for sized E-glass fibers [38]. This confirms validity of the baseline measurements. The rGF showed comparable strength values of 1.93 GPa and 1.74 GPa at 12 and 20 mm, respectively, with no statistically significant differences relative to vGF at any gauge length. This demonstrates that the methanolysis process does not induce measurable fiber strength degradation. The rGF-washed showed similar values (1.81 and 1.78 GPa at 12 and 20 mm), and while a slightly lower mean strength was observed relative to rGF at 4 mm (1.92 vs. 2.19 GPa; $p = 0.045$), this difference was absent at longer gauge lengths. Given that short gauge lengths are more sensitive to localized surface condition, this effect is likely attributable to the residual Na-rich deposits rather than bulk fiber degradation. Young's modulus was fully retained in all groups. At 12 mm, mean values were 70.8, 72.8, and 74.0 GPa for vGF, rGF, and rGF washed, respectively; at 20 mm, values were 71.4, 72.3, and 72.7 GPa — all within the accepted range for E-glass (70–80 GPa) [40]. Although a statistically significant difference was found between vGF and rGF washed at 12 mm ($p = 0.009$), no such difference was observed at 20 mm, and the absolute difference in mean values remained small (~4 GPa, <6%). This isolated result is thus not considered indicative of systematic stiffness degradation. Fiber diameter (13–15 μm) and strain at failure (2.3–3.4%) were consistent across all groups and gauge lengths, with no statistically significant differences observed. Taken together with the retained tensile strength and Young's modulus, these results indicate that no mechanically significant alkaline degradation occurred under the applied methanolysis conditions, consistent with the absence of severe surface pitting or etching observed by SEM. Since the tensile strength of glass fibers is highly sensitive to surface flaws, the absence of measurable strength loss provides an additional indirect indication that the finite alkaline treatment did not cause substantial surface damage.

To further assess the strength distribution and reliability of the fibers, Weibull statistical analysis (see Supporting Information) was performed on the 12 mm gauge length data (Fig. S17). The vGF showed a characteristic strength of $\sigma_0 = 2.08$ GPa and a Weibull modulus of $m = 6.97$, consistent with well-characterized sized E-glass fibers [41]. Strikingly, the rGF retained a comparable characteristic strength ($\sigma_0 = 2.13$ GPa), confirming that methanolysis does not reduce the intrinsic load-bearing capacity of the fibers. However, the Weibull modulus decreased to $m = 4.09$, reflecting an increased variability in strength and a broader distribution of critical flaws. This coincides with the increased surface roughness and heterogeneity observed after methanolysis, which may contribute to greater scatter in fiber strength without systematically reducing the mean strength. However, the present results do not establish a direct relationship between the chemical nature of the Na-rich deposits and individual fracture-initiation sites. Remarkably, following a simple ultrasonic washing with acetone, the Weibull modulus recovered to $m = 6.20$, while the σ_0 was 1.91 GPa. This suggests that the increased variability in rGF primarily originates from removable heterogeneity caused by surface contamination rather than irreversible structural damage. A comparison of the Weibull parameters (Table S11) shows that the rGFs recycled by our protocol exhibit a characteristic strength substantially higher than that of both conventionally pyrolyzed fibers (σ_0 = 0.94–1.24 GPa) and microwave-pyrolyzed fibers ($\sigma_0 = 1.00$–1.63 GPa). While mechanically ground fibers may retain relatively high characteristic strength (σ_0 = 2.47–2.85 GPa), their Weibull modulus is markedly lower ($m = 2.94$–4.22), indicating a broad and less reliable strength distribution that limits suitability for structural applications [38,41,42]. In contrast, our rGF-washed achieves both a characteristic strength and a Weibull modulus similar to that of the vGF baseline, indicating a

combination of high intrinsic strength and improved reliability.

These results demonstrate that methanolysis enables effective recovery of glass fibers while preserving their intrinsic mechanical properties. This can be attributed to the mild operating conditions of the process. Unlike pyrolysis, which exposes fibers to temperatures exceeding 400 °C and causes irreversible strength loss through thermally induced surface damage [38,42], methanolysis operates at moderate temperatures, chemically deconstructing the epoxy matrix without subjecting the fibers to the thermal stresses responsible for property degradation. The present approach therefore maintains both strength and statistical reliability, producing recycled fibers with performance close to that of virgin material and making them suitable candidates for high-value structural composite applications. To further assess the applicability of the liquefaction process to post-consumer or post-industrial composite waste, we subjected a trailing edge section from a decommissioned wind turbine blade (WTB) to our methanolysis process. TGA revealed roughly 1 wt% of residual content on the fiber after methanolysis (Fig. S18), confirming effective matrix removal from real blade waste. SEM examination further showed that the recovered WTB fibers retained a generally smooth surface without severe pitting or etching, although isolated surface deposits were still visible (Fig. S19). Point EDS analysis of a representative deposited region detected the characteristic glass-forming elements Si, Ca, Al and O, together with Na and C signals, indicating the presence of localized Na-containing and resin residues similar to those observed for the model rGF. Single-fiber tensile testing showed the expected decrease in strength with increasing gauge length, from approximately 2.1 GPa at 4 mm to 1.7 GPa at 12 mm and 1.3 GPa at 20 mm (Fig. 5). The Young's modulus remained high at approximately 77–80 GPa. Weibull analysis at 12 mm gave a characteristic strength of $\sigma_0 = 1.89 \pm 0.07$ GPa and a Weibull modulus of $m = 4.05 \pm 0.45$ (Fig. S20). The Weibull modulus is very close to that of the model rGF ($m = 4.09 \pm 0.36$), indicating a comparable degree of strength scatter, while the characteristic strength is somewhat lower than that of the model rGF. Importantly, this difference cannot be attributed solely to methanolysis, since the WTB fibers originate from a different commercial fiber system and have undergone composite manufacturing, long-term service and end-of-life pre-processing, while their unrecycled single-fiber properties are unavailable as a direct baseline. Nevertheless, the retention of GPa-level tensile strength and a Young's modulus close to typical E-glass values demonstrates that the methanolysis process can recover mechanically valuable glass fibers not only from the model GFRP but also from real end-of-life wind turbine blade waste.

2.4. Life cycle assessment of base-mediated methanolysis of GFRPs

We conducted a screening life cycle assessment (LCA) to estimate the global warming potential (GWP) and other environmental impacts of this waste treatment pathway. This assessment allows to compare this waste management option with other options, like the default disposal of WTB in landfills. The LCA methodology (see Supplementary Information for details) resulted in 16 default impact categories: climate change, acidification, freshwater ecotoxicity, particulate matter, marine, freshwater and terrestrial eutrophication, cancer and non-cancer human toxicity, ionising radiation, land use, ozone depletion, photochemical ozone formation, fossil and mineral/metal resource use and water use. The system boundary of this LCA is set as cradle-to-gate, which means that the impact of the use phase and end-of life of products coming out of the recycling process are not considered. Nonetheless, the impacts of chemicals and energy inputs needed for the treatment of the GFRP, and the impact of the residual waste streams from the process are considered. The Functional Unit, which forms the basis of comparison for the environmental impact, is the treatment of 1 kg GFRP derived from EOL WTB. A simplified process illustrating the core impact factors (input of chemicals and energy, and waste generated) that were included in the analysis is shown in Fig. 6 and Fig. S21, while more detailed data can be found in the Supplementary Information.

The environmental impact of processing 1 kg of GFRP waste is estimated in Table S13, while the relative contribution of different parameters influencing this environmental impact is shown in Fig. S22. From this comparison, it is clear that in most categories, the environmental footprint of the electricity used in the process is a determining factor. Also, the overall methanol consumption, both purging (as incineration with energy recovery) and use (especially with regards to the climate change category) is of extreme importance, hinting at the need for systems where a high polymer loading during the process is employed. To explore this further, additional calculations were performed for higher concentrations of waste in the solvent, which resulted in higher energy efficiency and lower net methanol consumption and losses. Higher waste loadings in methanolysis processes have in fact been achieved for other plastic streams, with a positive influence on the overall environmental performance by improving process intensification and reducing solvent-related impacts [29]. This results in a lower environmental impact for

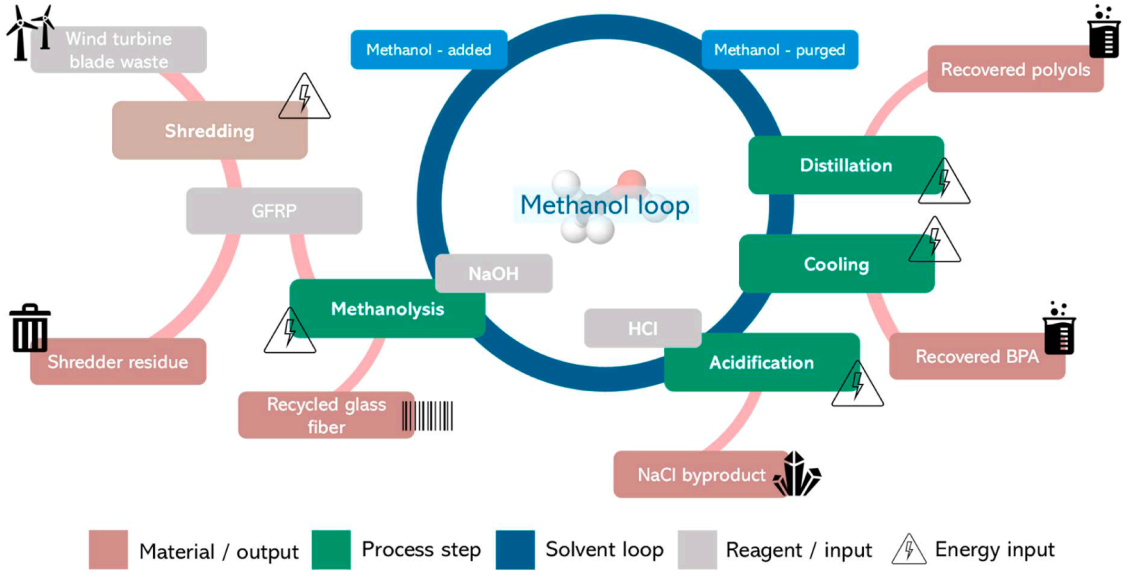


Fig. 6. Simplified process flow showing the parameters included in the environmental footprint calculation.

the process, and a higher relative contribution of NaOH and HCl to the environmental footprint (Figs. S23, S24 and Tables S14, S15). Importantly, the LCA includes the production and consumption of both NaOH and HCl as well as the generation of the resulting sodium salt stream formed during BPA recovery. Although NaOH is an inexpensive and widely available reagent, its relatively high loading represents an important contributor to the material footprint of the process, particularly at higher feed concentrations where the relative importance of energy demand decreases. In the current process configuration, acidification of the product stream generates NaCl. No NaOH regeneration loop was considered in the present assessment, representing a conservative scenario. At industrial scale, implementation of sodium recovery strategies, such as causticization, electrochemical regeneration, or reuse of alkaline liquors following product separation, could substantially reduce both reagent consumption and waste generation, thereby further improving the environmental performance of the recycling process. Similarly, methanol recovery via distillation was included through the solvent-recovery assumptions. Because methanol consumption was identified as a major contributor to several impact categories, high solvent recovery efficiencies are expected to be essential for industrial implementation. The present screening LCA did not explicitly model the design and energy requirements of a dedicated distillation train, but these requirements are indirectly reflected through the process energy demand considered in the assessment. Future process development should therefore focus on optimizing solvent-recovery efficiency and reducing solvent losses.

Evidently, the aim of the process is the recovery of valuable chemicals and materials. Therefore, one should not only assess the environmental impact of the recovery process but also take into account the avoided impacts of producing the recovered chemicals and materials from virgin resources. These are listed in Table S16. When subtracting these avoided impacts from the process impact, the net environmental footprint of the recycling process is obtained (Table 1). Negative values point to a net avoided impact, whereas positive values indicate impact categories where environmental impacts are not levelled out by the recovery of products and materials. In this case, the recycling system contributes to net benefits for the impact categories: acidification, particulate matter, marine eutrophication, human toxicity (non-cancer) and mineral resource use. These avoided impacts mainly come from the avoided virgin production of glass fiber (Table S16). When compared to disposing 1 kg GFRP in a sanitary landfill, benefits of the recycling route are obviously related to the same impact categories. For all other impact categories, the footprint of inert landfilled waste is lower than that of the recycling route. Naturally, for the scenario where a higher concentration of waste is used in the recycling process, the net environmental impact decreases, and becomes also beneficial (negative) for other categories, namely, climate change, freshwater ecotoxicity, land use, ozone depletion, photochemical ozone formation, fossil resource use and water use.

Circular economy measures typically minimize waste and improve resource efficiency by extending product lifespans and reincorporating materials into productive use. Considering avoided burden in the impact analysis of these measures is therefore crucial [43]. When materials are recovered through recycling or repurposing rather than landfilled, upstream processes such as mining, ore refinement, and virgin material production can be partially or completely avoided. Our environmental impact calculations illustrate that avoided impacts in a recycling system do not necessarily compensate for all impacts of the recycling process itself. In our case, for example, the overall climate impact in the default setup was not zero and remains higher than the landfilling option. Nevertheless, for other categories, such as mineral resource use, toxicity, eutrophication, and acidification, the net system-level impact is lower than for landfilling. Furthermore, since electricity represents a significant share of the environmental footprint, improving the energy efficiency of the recycling process is essential. This is clearly illustrated when comparing the default process with the setup using more concentrated feeds, as in the latter net environmental benefits increased due to lower energy demand. In addition, and often beyond the control of recycling operators, the composition of the electricity mix strongly influences the results. The environmental impact of the recycling system largely depends on how the consumed electricity is generated. In this study, the Belgian electricity mix was used, which includes a considerable share of nuclear and renewable energy (wind and solar). Applying a different energy mix would yield different results: French electricity, for example, is largely generated from nuclear energy and therefore results in a lower climate impact, while Dutch electricity is still largely derived from fossil sources, leading to a higher impact. A sensitivity analysis shows that, for this case, the global warming potential of the recycling process ranges from 5.68 kg CO_2-eq/kg GFRP (French mix) to 10.72 kg CO_2-eq/kg GFRP (Dutch mix), compared to 7.05 kg CO_2-eq/kg GFRP for the Belgian mix (Table S13). This demonstrates that variations due to

Table 1
Net impacts of the recycling system and comparison the landfill scenario.

Impact category	Unit	Treatment of waste (5 wt%)	Treatment of waste (50 wt%)	Credits for recycling output	Net result (5 wt%)	Net result (50 wt%)	Landfilling plastic waste (comparison)
Acidification	**mol H^+ eq**	1.06E-02	3.17E-03	−1.60E-02	**−5.33E-03**	**−1.28E-02**	**4.38E-05**
Climate change	**kg CO_2 eq**	7.05E+00	1.50E+00	−2.72E+00	4.33E+00	**−1.22E+00**	6.26E-03
Ecotoxicity, freshwater	**CTUe**	3.43E+01	1.15E+01	−1.61E+01	1.82E+01	**−4.63E+00**	1.11E-02
Particulate matter	**disease inc.**	7.89E-08	2.31E-08	−1.26E-07	**−4.74E-08**	**−1.03E-07**	**1.01E-09**
Eutrophication, marine	**kg N eq**	2.81E-03	7.17E-04	−3.26E-03	**−4.51E-04**	**−2.54E-03**	**1.67E-05**
Eutrophication, freshwater	**kg P eq**	1.31E-04	4.40E-05	−7.37E-05	5.75E-05	**−2.97E-05**	6.12E-08
Eutrophication, terrestrial	**mol N eq**	3.08E-02	7.78E-03	−3.58E-02	**−4.97E-03**	**−2.80E-02**	**1.84E-04**
Human toxicity, cancer	**CTUh**	3.97E-09	2.79E-09	−1.56E-09	2.41E-09	1.23E-09	1.13E-12
Human toxicity, non-cancer	**CTUh**	4.29E-08	2.53E-08	−1.05E-07	**−6.23E-08**	**−8.00E-08**	**2.54E-11**
Ionising radiation	**kBq U-235 eq**	1.61E+00	3.29E-01	−8.25E-02	1.53E+00	2.46E-01	3.56E-05
Land use	**Pt**	1.74E+01	4.37E+00	−7.22E+00	1.02E+01	**−2.85E+00**	3.01E-01
Ozone depletion	**kg CFC11 eq**	2.61E-07	6.86E-08	−1.14E-07	1.47E-07	**−4.57E-08**	1.74E-10
Photochemical ozone formation	**kg NMVOC eq**	1.34E-02	3.08E-03	−1.20E-02	1.39E-03	**−8.96E-03**	6.63E-05
Resource use, fossils	**MJ**	1.94E+02	3.99E+01	−4.70E+01	1.47E+02	**−7.05E+00**	1.53E-01
Resource use, minerals and metals	**kg Sb eq**	1.93E-05	7.09E-06	−2.09E-04	**−1.90E-04**	**−2.02E-04**	**9.16E-09**
Water use	**m^3 depriv.**	1.49E+00	3.75E-01	−6.22E-01	8.69E-01	**−2.47E-01**	6.68E-03

this single factor can be rather significant. Because electricity consumption represents the dominant contributor to the climate-change impact of the recycling process, further decarbonization of the electricity supply through increased penetration of wind and photovoltaic generation would be expected to reduce the global warming potential proportionally. Although dedicated renewable-electricity scenarios were not explicitly modelled in the present screening LCA, the comparison between the low-carbon French electricity mix and the more carbon-intensive Dutch electricity mix demonstrates the strong sensitivity of the results to the carbon intensity of electricity generation. These findings suggest that future deployment of the process in regions with highly renewable electricity systems could further improve its environmental performance, particularly with respect to climate-change impacts.

It should be also noted that the methanolysis energy demand used in the LCA was estimated based on operation under the experimentally determined reaction conditions, including the pressure conditions employed in this study. While elevated Ar pressure improved BPA recovery by suppressing methanol volatilization, alternative process configurations based on higher reactor filling ratios and autogenous pressure may provide similar benefits while reducing the need for external gas pressurization. Evaluation of such strategies was beyond the scope of the present work and should be addressed in future techno-economic and process-scale LCA studies. In addition to energy efficiency, material efficiency is also key. Solvent recovery is essential, as without high recovery rates, the environmental impacts of the recycling process would not be compensated by the credits for avoided burdens. Finally, the quality of the recovered products and materials is important. Environmental credits for recycled glass fibre, NaCl, BPA, and polyols can only be fully allocated if the quality is comparable to that of virgin materials. If this is not the case, more advanced approaches must be applied, using correction factors for quality loss [41]. Screening LCA is a useful tool to identify environmental hotspots, demonstrate the benefits of recycling systems, and identify opportunities for further improvement. The absolute values reported in this study should be considered indicative, as they are largely based on generic background datasets from the Ecoinvent database. For some parameters, such as methanol purging and incineration or the landfilling of residues, proxy data were used. More detailed studies would be required to obtain more accurate quantitative results.

3. Conclusion

In summary, we introduced a base-mediated alcoholysis strategy for epoxy thermoset deconstruction that combines operational simplicity with mechanistic insight into polymer accessibility and reactivity. This approach enables efficient depolymerization and monomer recovery under comparatively mild conditions using an inexpensive and readily available base promoter. Molecular dynamics insights highlight the key role of polymer structure and amine curing agent in epoxy reactivity, with more flexible networks facilitating accessibility and cleavage of the C(alkyl)-O bond. The process was successfully extended to glass fiber-reinforced composites, demonstrating the potential for simultaneous recovery of both the monomer and reinforcing materials. A screening life cycle assessment identified key environmental hotspots and opportunities for further process improvement.

From an industrial perspective, the proposed process eliminates the need for transition-metal catalysts. The combination of high BPA yields, preservation of fiber mechanical properties, and successful demonstration on end-of-life wind turbine blade waste highlights the potential of the approach for integration into future composite recycling value chains. Nevertheless, further process development is required before large-scale reuse. Acetone washing was employed here as a laboratory-scale cleaning treatment, and follow-up scale-up work should evaluate more environmentally benign and scalable alternatives, such as aqueous washing or carefully controlled dilute-acid treatment, considering cleaning efficiency, fiber property retention, cost, and environmental impact. Long-term alkali durability should also be assessed for recycled fibers' applications involving prolonged alkaline exposure, such as cementitious materials. Moreover, preservation of the intrinsic single-fiber properties does not necessarily ensure equivalent performance after remanufacturing into a new composite. The original sizing layer is expected to be substantially altered or removed during methanolysis, and re-sizing may therefore be required for applications. Although suitable sizing chemistries are readily available, homogeneous application to the recovered fibers and the stage at which the sizing is applied are important considerations, since sizing influences fiber handling, dispersion, alignment, impregnation, and interfacial performance. The additional cleaning and re-sizing operations, together with their associated economic and life-cycle impacts, will therefore need to be assessed during future process scale-up.

Furthermore, the LCA results indicate that process intensification can substantially improve environmental performance, with operation at higher feed concentrations reducing climate-change impacts to -1.22 kg CO_2-eq after accounting for recycling credits, demonstrating the strong influence of process efficiency on sustainability. Nevertheless, two key engineering bottlenecks currently limit large-scale implementation. First, the relatively low solid loading employed in the present study increases the energy demand associated with solvent heating and handling, thereby reducing process productivity and reactor throughput. Second, methanol consumption and solvent losses constitute a major contributor to the environmental footprint and operating costs of the process. These limitations are closely connected, as low feed concentrations translate into larger solvent inventories and consequently higher solvent recovery requirements. Therefore, future research should focus on increasing composite loadings while maintaining efficient mass transfer, polymer swelling, and depolymerization kinetics. Process intensification strategies such as semi-continuous reactor operation and improved mixing concepts may enable substantially higher throughputs and waste-treatment capacities per reactor volume. In parallel, development of closed-loop solvent recovery systems with minimal methanol losses are essential to reduce both economic and environmental costs. Additional techno-economic assessment, solvent recycling studies, and pilot-scale validation will be required to determine achievable treatment capacities and quantify the overall cost reduction relative to current disposal and recycling technologies.

Overall, this work demonstrates that efficient thermoset deconstruction can be achieved without sophisticated catalytic systems and establishes catalyst accessibility within the polymer network as a critical design parameter for future recycling technologies. This study provides a foundation for the development of scalable and economically viable recycling routes for thermoset composites and end-of-life wind turbine blade waste.

4. Methods

4.1. Epoxy resin synthesis

The epoxy resins used in the depolymerization experiments were either synthesized in-house following a modified literature procedure [44] or supplied by Westlake Epoxy. In short, the BPA-JEFF thermoset was prepared by combining 10 g of bisphenol A diglycidyl ether (BADGE) with the required amount of JEFFAMINE D-230 polyetheramine (Jeff D230) in a 20 mL vial under vigorous stirring (Table S2). The resulting mixture was cast into a Teflon mold and pre-cured in a hot press at 90 °C for 15 min under a pressure of 1 metric ton to increase viscosity. Subsequently, the sample was fully cured at 130 °C for 2 h under 2 metric tons of pressure. While still warm, the cured epoxy plate was demolded, cut into the desired dimensions, and allowed to cool to room temperature. The resulting polymer was used directly without further purification. The remaining thermosets, namely BADGE-IPDA,

BADGE-mXDA, and the formulations based on bisphenol F diglycidyl ether (BFDGE) were supplied by Westlake Epoxy and used as received without further purification (Tables S2 and S3).

4.2. Depolymerization reactions

A 100 ml high-pressure batch reactor (Premex) was used for the solvolysis of epoxy resins. To this end, the reactor was filled with the polymer and solvent. Then, the required amounts of base promoter were added, and the reactor was sealed, pressurized with Ar, heated to the desired temperature and stirred at 750 rpm for a specific time. After completion of the reaction, the reactor was cooled down in a water bath and opened to collect the product mixture. The unreacted polymer was recovered by filtration and the conversion was calculated by comparing it to the original epoxy resin weight. The product mixture (filtrate) was analyzed by gas chromatography (GC-FID) using calibration curve to determine yield.

4.3. Computational details

Molecular structures of the BPA tetramers BPA-JEFF, BPA-IPDA and BPA-mXDA were prepared and preoptimized using Avogadro (the resulting PDB files are provided) [45]. Classical MD simulations were performed on these structures in the *NPT* ensemble using a Langevin thermostat with a friction constant of 1 ps^{-1} and a Monte Carlo barostat, as implemented in the OpenMM package 8.0 [46]. Simulations were performed at experimental conditions of 200 °C and 20 bar over 170 ns with 20 ns equilibration using a time step of 1 fs. Longer simulations of 450 ns did not display significant changes to the calculated properties. Snapshots were saved every 10 ps for postprocessing (mainly calculating the radius of gyration) using MDTraj [47]. For the three simulated tetramers, a single molecule was packed in a simulation box together with 3000 methanol molecules using Packmol [48]. Forcefield parameters for the -tetramers and methanol were obtained through the CHARMM General Force Field (CGENFF) [49–51]. Simulations including NaOH were attempted but were unreliable due to unphysical ion aggregation at low concentrations. This is a shortcoming of the CHARMM force field that has been reported before in the literature [52,53]. Solving this issue is considered beyond the scope of this work, since the main interest is the accessibility of the reactive C(alkyl)-O bond to the solvent.

CRediT authorship contribution statement

Carlos Marquez: Writing – review & editing, Writing – original draft, Visualization, Methodology, Investigation, Formal analysis, Data curation, Conceptualization. **Yixue Zhang:** Writing – review & editing, Writing – original draft, Methodology, Investigation, Formal analysis, Data curation. **Karolien Vanbroekhoven:** Funding acquisition, Conceptualization. **Marc Comi:** Writing – review & editing, Investigation, Funding acquisition, Conceptualization. **Jelle Vekeman:** Writing – review & editing, Writing – original draft, Methodology, Investigation, Formal analysis. **Frank De Proft:** Writing – review & editing, Investigation, Conceptualization. **Jan Jordens:** Writing – review & editing, Investigation. **Tom Rommens:** Writing – review & editing, Writing – original draft, Investigation. **Jan Ivens:** Writing – review & editing, Funding acquisition, Conceptualization. **Joey Abi Rizk:** Investigation, Data curation. **Elias Feghali:** Writing – review & editing, Funding acquisition, Conceptualization. **Kathy Elst:** Writing – review & editing, Funding acquisition, Conceptualization.

Declaration of competing interest

A patent application covering the methanolysis process described in this work has been filed by VITO, with C.M, E.F and K.E as inventors. The patent covers aspects of the depolymerization methodology and its application to thermoset epoxy resin and composite recycling. The rest of the authors declare no competing interests.

Acknowledgements

The authors would like to acknowledge the financial support from the Flemish Government and Flanders Innovation & Entrepreneurship (VLAIO) through the Moonshot project (CYCLOPS HBC.2021.0584). This research was also carried out as part of the WIN-CE project (HBC.2023.1006), a strategic basic research (cSBO) initiative conducted within the Flemish spearhead clusters Catalisti and De Blauwe Cluster and supported by Flanders Innovation & Entrepreneurship (VLAIO). The computational resources and services used in this work were provided by the VSC (Flemish Supercomputer Center), funded by the Research Foundation-Flanders (FWO) and the Flemish Government. The authors acknowledge Peter De Rechter (VITO) for his support in GC analyses. The authors are grateful to Dr. Christoph Schädle and Westlake Epoxy for preparing and providing us the epoxy-based resins with different curing agents used in this work.

Supplementary materials

Supplementary material associated with this article can be found, in the online version, at doi:10.1016/j.rineng.2026.112930.

Data availability

Data will be made available on request.

References

[1] H.Q. Pham, M.J. Marks, Ullmann's Encyclopedia of Industrial Chemistry, Wiley-VCH Verlag GmbH & Co. KGaA, Weinheim, 2005.
[2] R.C. DiPucchio, K.R. Stevenson, C.W. Lahive, W.E. Michener, G.T. Beckham, Base-mediated depolymerization of amine-cured epoxy resins, ACS Sustain. Chem. Eng. 11 (2023) 16946–16954, https://doi.org/10.1021/acssuschemeng.3c04181.
[3] S.R. Nicholson, N.A. Rorrer, A.C. Carpenter, G.T. Beckham, Manufacturing energy and greenhouse gas emissions associated with plastics consumption, Joule 5 (2021) 673–686, https://doi.org/10.1016/j.joule.2020.12.027.
[4] N. Papadakis, C. Ramírez, N. Reynolds, Designing composite wind turbine blades for disposal, recycling or reuse, in: V. Goodship (Ed.), Management, Recycling and Reuse of Waste Composites, Woodhead Publishing, Sawston, UK, 2010, pp. 443–457.
[5] E. Linak, U. Buchholz, M. Guan, A. Kishi, IHS Report On Epoxy Resins, IHS Markit, 2020.
[6] J. Zhang, G. Lin, U. Vaidya, H. Wang, Past, present and future prospective of global carbon fibre composite developments and applications, Compos. B Eng. 250 (2023) 110463, https://doi.org/10.1016/j.compositesb.2022.110463.
[7] L. Zhu, N. Li, P.R.N. Childs, Light-weighting in aerospace component and system design, Propuls. Power Res. 7 (2018) 103–119, https://doi.org/10.1016/j.jppr.2018.04.001.
[8] W. Zhang, J. Xu, Advanced lightweight materials for automobiles: a review, Mater. Des. 221 (2022) 110994, https://doi.org/10.1016/j.matdes.2022.110994.
[9] T. Yildiz, Design and analysis of a lightweight composite shipping container made of carbon fiber laminates, Logistics 3 (2019) 18, https://doi.org/10.3390/logistics3030018.
[10] J. Zhang, V.S. Chevali, H. Wang, C.-H. Wang, Current status of carbon fibre and carbon fibre composites recycling, Compos. B Eng. 193 (2020) 108053, https://doi.org/10.1016/j.compositesb.2020.108053.
[11] H. Sun, A. Ahrens, G.M.F. Batista, B.S. Donslund, A.K. Ravn, E.V. Schwibinger, A. Nova, T. Skrydstrup, Solvent–base mismatch enables the deconstruction of epoxy polymers and bisphenol A recovery, Green Chem. 26 (2024) 815–824, https://doi.org/10.1039/d3gc03707j.
[12] M. Diani, M. Colledani, Energy consumption assessment and modeling of a comminution process: the glass fibers reinforced composites case-study, Procedia CIRP 90 (2020) 483–487, https://doi.org/10.1016/j.procir.2020.01.117.
[13] A.E. Krauklis, C.W. Karl, A.I. Gagani, J.K. Jørgensen, Composite material recycling technology—state-of-the-art and sustainable development for the 2020s, J. Compos. Sci. 5 (2021) 28, https://doi.org/10.3390/jcs5010028.
[14] HDIN Research, Wind turbine blade market analysis, accessed May, https://www.hdinresearch.com/reports/156307, 2026. accessed May.
[15] REN21, GSR 2025 factsheet: supply - wind, accessed May, https://www.ren21.net/gsr-2025/downloads/pdf/supply/GSR_2025_Factsheet_Supply_Wind.pdf, 2026. accessed May.
[16] S.K. Gopalraj, T.A. Kärki, A review on the recycling of waste carbon fibre/glass fibre-reinforced composites: fibre recovery, properties and life-cycle analysis, SN Appl. Sci. 2 (2020) 433, https://doi.org/10.1007/s42452-020-2195-4.

[17] C. Ma, D. Sánchez-Rodríguez, T. Kamo, A comprehensive study on the oxidative pyrolysis of epoxy resin from fiber/epoxy composites: product characteristics and kinetics, J. Hazard. Mater. 412 (2021) 125329, https://doi.org/10.1016/j.jhazmat.2021.125329.
[18] S.R. Naqvi, H.M. Prabhakara, E.A. Bramer, W. Dierkes, R. Akkerman, G. Brem, A critical review on recycling of end-of-life carbon fibre/glass fibre reinforced composites waste using pyrolysis towards a circular economy, Resour. Conserv. Recycl. 136 (2018) 118–129, https://doi.org/10.1016/j.resconrec.2018.04.013.
[19] P. Liu, C.Y. Barlow, Wind turbine blade waste in 2050, Waste Manag. 62 (2017) 229–240, https://doi.org/10.1016/j.wasman.2017.02.007.
[20] S.J. Pickering, Recycling technologies for thermoset composite materials—current status, Compos. A Appl. Sci. Manuf. 37 (2006) 1206–1215, https://doi.org/10.1016/j.compositesa.2005.05.030.
[21] G.N. Petropoulos, P. Tsokanas, A. Kotrotsos, V. Kostopoulos, Recycled glass fibre–epoxy composites based on recovered fabrics from an environment-friendly combined solvolysis and thermolysis route, Compos. Sci. Technol. 263 (2025) 111048, https://doi.org/10.1016/j.compscitech.2025.111048.
[22] G.N. Petropoulos, P. Tsokanas, C. Marquez, V. Kostopoulos, Eco-friendly recycling of CFRP composites via hydrogen peroxide treatment: preserving fabric architecture for second-life applications, Compos. Part A Appl. Sci. Manuf. 209 (2026) 109914, https://doi.org/10.1016/j.compositesa.2026.109914.
[23] A. Ahrens, A. Bonde, H. Sun, N.K. Wittig, H.C.D. Hammershøj, G.M.F. Batista, A. Sommerfeldt, S. Frølich, H. Birkedal, T. Skrydstrup, Catalytic disconnection of C–O bonds in epoxy resins and composites, Nature 617 (2023) 730–737, https://doi.org/10.1038/s41586-023-05944-6.
[24] Y. Huang, Y. Yamazaki, K. Nomoto, H. Miura, T. Shishido, X. Jin, K. Nozaki, Bimetallic synergy in supported Ni–Pd catalyst for selective hydrogenolysis of C–O bonds in epoxy resins, Nat. Commun. 16 (2025) 1188, https://doi.org/10.1038/s41467-025-56488-4.
[25] Y. Liao, K. Takahashi, K. Nozaki, Nickel-catalyzed C(sp3)-O hydrogenolysis via a remote-concerted oxidative addition and its application to degradation of a bisphenol A-based epoxy resin, J. Am. Chem. Soc. 146 (2024) 2419–2425, https://doi.org/10.1021/jacs.3c09061.
[26] Y.J. Lim, Z. Yu, V. Cherepakhin, T.J. Williams, S.R. Nutt, Fiber and monomer recovery from an amine-cured epoxy composite using molten NaOH–KOH, Green Chem. 27 (2025) 2184–2188, https://doi.org/10.1039/d4gc05299d.
[27] C.W. Lahive, S.H. Dempsey, S.E. Reiber, A. Pal, K.R. Stevenson, W.E. Michener, H. M. Alt, K.J. Ramirez, E.G. Rognerud, C.L. Lincoln, R.W. Clarke, J.S. DesVeaux, T. Uekert, N.A. Rorrer, K.M. Knauer, G.T. Beckham, Acetolysis for epoxy-amine carbon fibre-reinforced polymer recycling, Nature 642 (2025) 605–612, https://doi.org/10.1038/s41586-025-09067-y.
[28] S.S. Núñez, N. Ortuño, S. Fernández-Durán, J. Moltó, J.A. Conesa, Analysis and removal of bisphenols in recycled plastics using polyethylene glycol, Sci. Rep. 14 (2024) 12824, https://doi.org/10.1038/s41598-024-63800-7.
[29] D. Parida, A. Aerts, L.V. Perez, C. Marquez, S. Vloemans, K. Vanbroekhoven, E. Feghali, K. Elst, Boosting methanolysis of polycarbonate (PC) for bisphenol A recovery from end-of-life PC and PC/ABS blend, Chem. Eng. J. 497 (2024) 154390, https://doi.org/10.1016/j.cej.2024.154390.
[30] C. Marquez, A. Aerts, D. Parida, I. Glassee, H. Mitta, L. Li, K.M. Van Geem, K. Vanbroekhoven, E. Feghali, K. Elst, Monomer recycling of virgin polycarbonate (PC), end-of-life PC and PC-ABS blends by Ni-catalyzed reductive depolymerization, Green Chem. 27 (2025) 5709–5714, https://doi.org/10.1039/d4gc06438k.
[31] M.E. Pool, E. Savage, R. Holland, C.W. Lahive, M.P. Shaver, Chemical recycling of polycarbonate acrylonitrile butadiene styrene (PC/ABS) blends via organocatalyzed acetolysis, ChemSusChem 19 (2026) e202502161, https://doi.org/10.1002/cssc.202502161.
[32] A.I. Tkachuk, A.G. Zagora, I.V. Terekhov, R.R. Mukhametov, Isophorone diamine—a curing agent for epoxy resins: production, application, prospects. A review, Polym. Sci. Ser. D 15 (2022) 171–176, https://doi.org/10.1134/S1995421222020289.
[33] F. Fraga, C. Castro-Díaz, E. Rodríguez-Núñez, J.M. Martínez-Ageitos, Physical aging for an epoxy network diglycidyl ether of bisphenol A/m-xylylenediamine, Polymer 44 (2003) 5779–5784, https://doi.org/10.1016/S0032-3861(03)00624-4.
[34] S. Yamamoto, K. Tanaka, Molecular dynamics simulation of cross-linked epoxy resins: past and future, Macromol. Rapid Commun. 46 (2025) 2400978, https://doi.org/10.1002/marc.202400978.
[35] J. Fan, A. Anastassiou, C.W. Macosko, E.B. Tadmor, Molecular dynamics predictions of thermomechanical properties of an epoxy thermosetting polymer, Polymer 196 (2020) 122477, https://doi.org/10.1016/j.polymer.2020.122477.
[36] Y. Zhang, Y. Pontikes, J. van Caneghem, L. Lessard, A.W. van Vuure, Parametric analysis of inorganic polymers reinforced with recycled GFRP materials, Constr. Build. Mater. 463 (2025) 139986, https://doi.org/10.1016/j.conbuildmat.2025.139986.
[37] Y. Zhang, Y. Pontikes, L. Lessard, A.W. van Vuure, Recycling and valorization of glass fibre thermoset composite waste by cold incorporation into a sustainable inorganic polymer matrix, Compos. B Eng. 223 (2021) 109120, https://doi.org/10.1016/j.compositesb.2021.109120.
[38] A. Rahimizadeh, M. Tahir, K. Fayazbakhsh, L. Lessard, Tensile properties and interfacial shear strength of recycled fibers from wind turbine waste, Compos. A Appl. Sci. Manuf. 131 (2020) 105786, https://doi.org/10.1016/j.compositesa.2020.105786.
[39] A. Rahimizadeh, J. Kalman, R. Henri, K. Fayazbakhsh, L. Lessard, Recycled glass fiber composites from wind turbine waste for 3D printing feedstock: effects of fiber content and interface on mechanical performance, Materials 12 (2019) 3929, https://doi.org/10.3390/ma12233929.
[40] F.R. Jones, N.T. Huff, The structure and properties of glass fibres, in: A.R. Bunsell (Ed.), Handbook of Properties of Textile and Technical Fibres, Elsevier, 2018, pp. 757–803.
[41] F. Mesquita, S. Bucknell, Y. Leray, S.V. Lomov, Y. Swolfs, Single carbon and glass fibre properties characterised using large data sets obtained through automated single fibre tensile testing, Compos. A Appl. Sci. Manuf. 145 (2021) 106389, https://doi.org/10.1016/j.compositesa.2021.106389.
[42] Y. Zhang, S. Verschuere, J. Eliat-Eliat, J. Ivens, Feasibility study of a pre-swelling microwave-assisted recycling method for GFRP waste, J. Compos. Sci. 10 (2026) 71, https://doi.org/10.3390/jcs10020071.
[43] M. Kabir, M.H. Young, G. Gülen, S. Singh, Assessing avoided burden and net environmental impact by recycling and repurposing of retiring wind turbines, Environments 12 (2025) 396, https://doi.org/10.3390/environments12110396.
[44] M. Comí, M. Thys, A. Aerts, S. Geudens, S. Vloemans, E. Feghali, K. Vanbroekhoven, R. Vendamme, Revealing the dynamics of sustainable epoxy–acrylate networks from recycled plastics blends and oligomeric lignin precursors, ChemSusChem 18 (2025) e202402375, https://doi.org/10.1002/cssc.202402375.
[45] M.D. Hanwell, D.E. Curtis, D.C. Lonie, T. Vandermeersch, E. Zurek, G.R. Hutchison, Avogadro: an advanced semantic chemical editor, visualization, and analysis platform, J. Cheminform. 4 (2012) 17, https://doi.org/10.1186/1758-2946-4-17.
[46] P. Eastman, R. Galvelis, R.P. Peláez, C.R.A. Abreu, S.E. Farr, E. Gallicchio, A. Gorenko, M.M. Henry, F. Hu, J. Huang, A. Krämer, J. Michel, J.A. Mitchell, V. S. Pande, J.P.G.L.M. Rodrigues, J. Rodriguez-Guerra, A.C. Simmonett, S. Singh, J. Swails, P. Turner, Y. Wang, I. Zhang, J.D. Chodera, G. De Fabritiis, T. E. Markland, OpenMM 8: molecular dynamics simulation with machine learning potentials, J. Phys. Chem. B 128 (2024) 109–116, https://doi.org/10.1021/acs.jpcb.3c06662.
[47] R.T. McGibbon, K.A. Beauchamp, M.P. Harrigan, C. Klein, J.M. Swails, C. X. Hernández, C.R. Schwantes, L.-P. Wang, T.J. Lane, V.S. Pande, MDTraj: a modern open library for the analysis of molecular dynamics trajectories, Biophys. J. 109 (2015) 1528–1532, https://doi.org/10.1016/j.bpj.2015.08.015.
[48] L. Martínez, R. Andrade, E.G. Birgin, J.M. Martínez, Packmol: a package for building initial configurations for molecular dynamics simulations, J. Comput. Chem. 30 (2009) 2157–2164, https://doi.org/10.1002/jcc.21224.
[49] K. Vanommeslaeghe, A.D. MacKerell Jr., Automation of the CHARMM general force field (CGenFF) I: bond perception and atom typing, J. Chem. Inf. Model. 52 (2012) 3144–3154, https://doi.org/10.1021/ci300363c.
[50] K. Vanommeslaeghe, E.P. Raman, A.D. MacKerell Jr., Automation of the CHARMM general force field (CGenFF) II: assignment of bonded parameters and partial atomic charges, J. Chem. Inf. Model. 52 (2012) 3155–3168, https://doi.org/10.1021/ci3003649.
[51] CGenFF, accessed 13 May, https://cgenff.com/, 2026. accessed 13 May.
[52] J. Vekeman, D. Vandenabeele, N. Doppelhammer, E. Vandeurzen, E. Breynaert, C. E.A. Kirschhock, T. Verstraelen, Simple molecular model for hydrated silicate ionic liquids, a realistic zeolite precursor, Chem. Mater. 36 (2024) 3886–3897, https://doi.org/10.1021/acs.chemmater.4c00285.
[53] S. Blázquez, M.M. Conde, C. Vega, Scaled charges for ions: an improvement but not the final word for modeling electrolytes in water, J. Chem. Phys. 158 (2023) 054505, https://doi.org/10.1063/5.0136498.